JCTC Journal of Chemical Theory and Computation

Article

pubs.acs.org/JCTC

Enhancing Conformation and Protonation State Sampling of Hen Egg White Lysozyme Using pH Replica Exchange Molecular Dynamics

Jason M. Swails and Adrian E. Roitberg*

Quantum Theory Project, Chemistry Department, University of Florida, Gainesville, Florida 32611, United States

ABSTRACT: We evaluate the efficiency of the pH replica exchange molecular dynamics (pH-REMD) method proposed by Itoh et al. (*Proteins* **2011**, *79*, 3420−3436) by using it to predict the pK_a values of the titratable residues in hen egg white lysozyme (HEWL). pK_a values predicted using pH-REMD converge significantly faster than those calculated using constant pH molecular dynamics (CpHMD). Furthermore, increasing the frequency between exchange attempts in pH-REMD simulations improves protonation and conformational state sampling. By enabling the simulation to sample both conformational and protonation states more rapidly, pH-REMD simulations provide valuable insight into the pH-dependence of HEWL that the CpHMD simulations failed to capture. We present an efficient and highly scalable implementation of pH-REMD as an attractive enhancement to traditional CpHMD methods.

1. INTRODUCTION

Solution pH is often critical to the proper functioning of biological catalysts.[1−3] The pH environment of biological systems influences the ionization equilibria present in the system, thereby affecting the protonation state of various titratable residues in the system. A titratable residue is any residue that has a pK_a value within 1 or 2 units of the biological pH range (which is roughly 2−9). The protonation states of these residues can have a profound effect on the stability of the system, the system's interactions with its surroundings, and any catalytic mechanism that relies on a specific set of protonation states to carry out general acid−base catalysis or nucleophilic attack.[4]

Simulations aimed at modeling proteins or nucleic acids must have some method for assigning protonation states for each titratable residue. Because bond breaking and bond formation are impossible in classical force fields, each residue is typically assigned one protonation state, and the entire simulation is run using this set of states. This approach has two drawbacks. First, the choice of protonation state is often based on the behavior of each titratable residue when free in solution. This may not be a valid assumption, however, because the protein or nucleic acid environment can modulate a residue's protonation state equilibrium. Second, a single protonation state may not accurately represent the true ensemble of states at the desired pH. If the pH is close in magnitude to the pK_a of a given residue, or if the system populates conformations in which the dominant protonation state changes, then the true ensemble is represented by conformations with different protonation states.

The first drawback can be addressed by using tools such as PROPKA[5] and H++,[6] which provide a means to assign protonation states to titratable residues by calculating the pK_a of the starting structure. However, this does not address the possibility that multiple protonation states may be necessary to build the desired ensemble.

While it may seem that both drawbacks can be addressed by simply running simulations with every possible set of protonation states, this approach quickly becomes unwieldy. Given N titratable residues, there are 2^N distinct protonation states assuming each residue is either protonated or deprotonated. With only 10 titratable residues, this amounts to 1024 distinct simulations! While most of these states may not be found in the given ensemble, there is no way to know which ones to exclude a priori. It is important then to develop a method capable of directly probing protonation state equilibria in biological molecules.

To probe protonation state equilibria in a thermodynamically meaningful way, simulations must be run at constant pH. The first approaches for constant pH simulations used continuum electrostatics methods to calculate the perturbing effect of the system environment on protonation state equilibria using an implicit solvent model (e.g., the Poisson−Boltzmann equation) on a single structure.[7−9] These methods, while sometimes useful for calculating pK_a values in biological systems, assume that the full protonation state equilibria can be characterized with a single structure. In particular, using a single structure neglects the response of the system relaxing to accommodate the new protonation state. While this has been addressed to some degree by treating the protein interior with a large dielectric constant,[9] this approach assumes an unphysical homogeneity in the system's dielectric response to protonation state changes.

A more sophisticated approach to incorporating the system response involves simultaneous sampling of both protonation states and side-chain rotamers.[10] This approach dramatically improves pK_a prediction with respect to experiment, but may be insufficient for systems with large-scale conformational changes that cannot be attributed only to side-chain mobility.

To capture the coupled nature of conformational flexibility with protonation state sampling, several constant pH molecular dynamics (CpHMD) methods have been proposed.[11−17] These

Received: June 20, 2012
Published: August 29, 2012

methods have proven to be powerful tools for pK_a calculation and prediction, although there is still room for improvement.[18] For systems in which some titratable residues experience large pK_a shifts, predicted pK_a values are often in error by more than 1 pH unit even in the studies that reproduce experimental values the closest.[18] This is usually a direct result of insufficient sampling of protonation and conformational states or a limitation of the underlying model. Machuqueiro and Baptista have shown that correcting some of the limitations of the underlying model, such as improving the definition of the reference compound (whose role is described in the Theory) and improving the underlying force field, improves results.[19] Other work has coupled enhanced sampling techniques, such as accelerated molecular dynamics,[20] with CpHMD to show that improved conformational sampling also improves predicted pK_a's with respect to experiment.[21] Webb et al. recently published a systematic study showing that the errors inherent to experimental measurements are often larger than those reported, which has important implications for the accuracy of theoretical predictions.[22]

Replica exchange molecular dynamics (REMD) is a family of extended ensemble techniques that have been shown to dramatically improve sampling.[23−28] In REMD simulations, a series of independent replicas (single MD trajectories of a system) periodically attempt to exchange information, such as temperature[23,24] and, more recently, pH,[1,29] to sample from an expanded ensemble covering multiple states.

In this study, we implemented, in the *sander* module of the AMBER[30] software package, the pH-REMD method described by Itoh et al.[1] We show how this method significantly improves sampling as compared to CpHMD in hen egg white lysozyme (HEWL), a system commonly used as a benchmark for pK_a calculations. Titration curves generated using pH-REMD contain significantly less noise and converge more rapidly than CpHMD, suggesting pH-REMD is a powerful tool for carrying out pK_a predictions.

Our group has previously shown that temperature REMD simulations converge significantly faster with increasing exchange attempt frequency (EAF).[31,32] Here, we show that increasing the EAF in pH-REMD simulations causes pH-dependent observable properties to converge faster as well.

This Article is divided into the following sections: In the Theory, we first discuss the foundation of the constant pH method developed by Mongan et al.[16] and the corresponding pH-REMD method.[1,29] In the Methods, we explain the details of the CpHMD and pH-REMD simulations performed on HEWL. Finally, in the Results and Discussion, we highlight the successes of pH-REMD as compared to CpHMD and how modifications made to the exchange attempt process can further enhance the performance of pH-REMD.

2. THEORY

Before discussing the details of the simulations, we will describe the theory behind the two methods we used in this study: CpHMD and pH-REMD.

2.1. CpHMD. We used the constant pH molecular dynamics (CpHMD) method developed by Mongan et al.[16] that employs Monte Carlo transitions between discrete protonation states at periodic intervals during a MD simulation to probe protonation state equilibria. In this CpHMD implementation, both the dynamics and the MC protonation state sampling are performed in Generalized Born implicit solvent. After a predetermined number of steps, the MD is halted and a protonation state change is attempted by evaluating the energetic cost of that proposed change, calculated according to[16]

$$\Delta G = k_B T(\mathrm{pH} - \mathrm{p}K_{a,\mathrm{ref}}) \ln 10 + \Delta G_{\mathrm{elec}} - \Delta G_{\mathrm{elec,ref}} \quad (1)$$

Equation 1 represents a free energy change of protonating or deprotonating a titratable residue embedded in a biological system with respect to a predefined reference compound. The reference compound is a monomer of the titratable residue capped with small, neutral functional groups. In eq 1, ΔG_{elec} is calculated by taking the difference of the electrostatic energy between the proposed and existing protonation states.[16]

Directly calculating the free energy change associated with protonation or deprotonation is difficult because evaluating the energetic cost of desolvating a free proton and making and breaking chemical bonds is impossible in a classical mechanical framework. Therefore, we calculate the free energy cost of this protonation state change by comparing the free energy of the protonation state change to $\Delta G_{\mathrm{elec,ref}}$ in eq 1, a precomputed free energy for the reference compound that is adjusted to reproduce experimental pK_a values. Equation 1 then represents a shift in the pK_a of a titratable residue in a biological system from its value free in solution. The reference compound pK_a values used in the AMBER CpHMD implementation[16] are shown in Table 1.

Table 1. Reference pK_a Values for the Acidic Residues Treated in This Study[a]

residue	reference pK_a
aspartate	4.0
glutamate	4.4
histidine (H^{δ})	7.1
histidine (H^{ϵ})	6.5

[a]Values are the same as those used in the original AMBER CpHMD implementation.[16]

Running a CpHMD simulation, we obtain an ensemble consisting of multiple protonation states properly weighted for the semigrand canonical ensemble, the thermodynamic ensemble corresponding to constant temperature, volume (or pressure), and chemical potential of hydronium (i.e., constant pH).[12] Because the simulation is assumed to be ergodic, the deprotonation fraction can be calculated by simply counting the fraction of ensemble members in which the residue is deprotonated. Multiple CpHMD simulations must be run with a range of pH's to calculate pK_a values for titratable residues in biological systems by fitting a titration curve to the data.

Running a simulation with an expanded ensemble so each CpHMD simulation is in equilibrium with simulations at different pH's can further enhance sampling from the desired semigrand canonical ensemble. For this, we turn to the pH-REMD method.

2.2. pH-REMD. Replica exchange simulations at constant pH (pH-REMD) are a variant of replica exchange in which each replica is simulated at a separate pH. The full pH-REMD simulation represents an expanded ensemble in which each replica samples conformations with a fixed pH and samples different pH values at a fixed conformation.

In this study, we implemented the pH-REMD method introduced by Itoh et al.[1] in the *sander* module of AMBER.[30] In

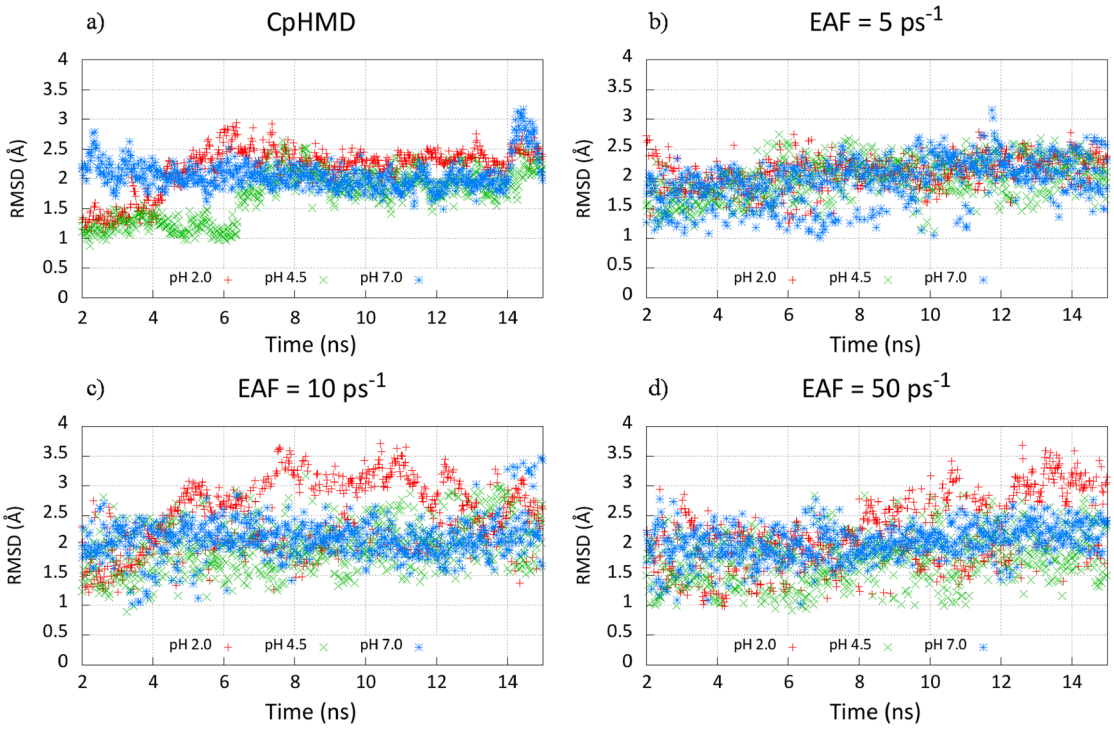

Figure 1. The RMSD plots for CpHMD simulations (a) and pH-REMD simulations at different exchange attempt frequencies (b–d) as a function of time throughout the simulation. The first nanosecond is excluded, as described in Methods. The RMSD is plotted with respect to the minimized crystal structure 1AKI and is shown for one low, one medium, and one high pH simulation (2, 4.5, and 7, respectively).

pH-REMD, adjacent replicas in the pH ladder swap pH with the Monte Carlo exchange probability:

$$P_{i\rightarrow j} = \min\{1, \exp[\ln 10(N_i - N_j)(\mathrm{pH}_i - \mathrm{pH}_j)]\} \quad (2)$$

for replicas i and j where N_i is the number of titratable protons present in replica i and $p\mathrm{H}_i$ is the pH of replica i prior to the exchange attempt.

Our group recently developed a different pH-REMD method in which replica exchanges are attempted via Hamiltonian exchange where only atomic coordinates are swapped.[33] In contrast, the currently proposed method only swaps the solution pH between replicas. For large systems with more than 3–5 titratable residues, the proposed method of swapping solution pH between replicas achieves more efficient replica exchanges than the variant employing Hamiltonian exchange. For HEWL, specifically, the Hamiltonian REMD variant experienced an exchange attempt success rate of <0.01%, which is effectively indistinguishable from CpHMD simulations.

3. METHODS

3.1. Starting Structure. We chose to study hen egg white lysozyme because it is well-characterized both experimentally[22,34,35] and computationally.[16,29,36] We chose the structure from the protein data bank (PDB) with the code 1AKI[37] because it was the focus of Mongan's original study.[16]

The topology file was prepared in the *tleap* module of AmberTools 12 using the AMBER *ff10* force field, which is equivalent to *ff99SB*[38] for proteins. Crystallographic water molecules were removed from the starting structures, and *tleap* added all hydrogen atoms. Finally, the *mbondi2* intrinsic radii for implicit solvent calculations were selected in *tleap* to be consistent with the initial implementation of CpHMD.[16]

3.2. Molecular Dynamics. To be consistent with the original implementation, the Generalized Born model described by Onufriev et al.[39] (corresponding to the input parameter *igb=2* for AMBER programs) was used with the salt concentration, modeled as a Debye screening parameter, set to 0.1 M in every simulation.[16] Because of the long-range nature of the electrostatic forces, we always used an infinite cutoff for nonbonded interactions.

Each starting structure was minimized using 50 steps of steepest descent followed by 950 steps of conjugate gradient with 10 kcal mol^{-1} Å^{-2} restraints on the backbone atoms to relieve bad contacts. Next, the minimized structure was heated by varying the target temperature linearly from 10 to 300 K for 667 ps, keeping weak restraints, 1 kcal mol^{-1} Å^{-2}, on the backbone. We used the Langevin thermostat with a collision frequency of 5 ps^{-1} to control the temperature. These simulations were performed using the *pmemd* module of the AMBER 12 program suite.[30]

After heating, each structure was further run at 300 K for 1 ns with 0.1 kcal mol^{-1} Å^{-2} restraints on the backbone. Each titratable carboxylate was deprotonated and the histidine was protonated, and no protonation state changes were attempted during the simulation. Next, the resulting structure was used to start 16 ns of CpHMD at pH values spanning 2–7 with an interval of 0.5. Only the 10 acidic residues, the aspartates, glutamates, and histidines, were titrated because HEWL is catalytically active at low pH,[40] and all 1AKI were solved in these conditions. We used a 2 fs time step and attempted protonation state changes every 5 steps. The Langevin thermostat with a collision frequency of 10 ps^{-1} was used to control the temperature, and simulations were begun with a different random seed to avoid synchronization artifacts.[41] We used the *sander* module of AMBER 12 for each of these simulations.

dx.doi.org/10.1021/ct300512h | J. Chem. Theory Comput. 2012, 8, 4393–4404

3.3. Replica Exchange. All pH-REMD simulations were run with 12 equally spaced replicas at pH values spanning 2–7.5, identical to the pH values used for the CpHMD simulations with the addition of a replica at pH 7.5. The additional replica is necessary because the REMD implementation in *sander* requires an even number of replicas so that each replica has a partner for each exchange attempt. The structures obtained after 1 ns of CpHMD simulation for each pH were used as the starting structure for the replica exchange simulations (the structure from CpHMD run at pH 7 was used for the replica run at pH 7.5 as well).

We ran pH-REMD simulations with exchange attempt frequencies (EAFs) (i.e., the frequency with which replicas attempt to swap pH values) equal to 50, 10, 5, and 0.5 ps^{-1} to assess the effect of EAF on the convergence of observable properties. This corresponds to attempting exchanges every 10, 50, 100, and 1000 steps, respectively. All pH-REMD simulations were run for 15 ns. We note here that the CpHMD simulations are equivalent to a REMD simulation with an EAF equal to 0.

We used an in-house, modified version of *sander* in which we implemented pH-REMD for these simulations and wrote in-house scripts to extract pH-based titration data from the ensemble of replica-based files. The replica at pH 7.5 was ignored in all pH-REMD analyses so the simulations could be compared fairly.

4. RESULTS AND DISCUSSION

CpHMD methods must sample both protonation states and conformation states to build a thermodynamically meaningful ensemble. Here, we will discuss how well CpHMD, as implemented in AMBER,[16] samples from the desired ensemble. We then analyze how pH-REMD affects protonation and conformational state sampling as compared to CpHMD, and how effective these tools are for pK_a prediction.

4.1. Simulation Stability. CpHMD involves instantaneous changes in the charge distribution of the protein as the protonation states are changed. Therefore, it is important to verify that trajectories generated from CpHMD and pH-REMD remain stable with respect to secondary and tertiary structure during the course of the simulation.

Mongan et al.[16] showed that temperature and energy fluctuations greater than those obtained with standard MD (i.e., MD simulations with static protonation states) were minimal during the course of a 1 ns simulation. Most of the energy fluctuations arise from the intrinsic response of the force field to the new charge state.

To analyze structural stability, we plotted the root mean squared deviation (RMSD) of every α-carbon in the protein with respect to the minimized crystal structure versus time. The results from CpHMD and pH-REMD simulations are shown in Figure 1 for the lowest pH, 2; the highest pH, 7; and an intermediate pH, 4.5. The RMSDs are bounded below 4 Å, suggesting that the trajectories remain stable for both CpHMD and pH-REMD during the entire simulation.

4.2. Accuracy of Predicted pK_a's. One of the goals of any constant pH simulation method is to accurately predict pK_a values of titratable residues. The pK_a of each residue was calculated by using the Levenberg–Marquardt nonlinear optimization method to fit the titration data at each pH to the standard Hill equation shown below:

$$f_d = \frac{1}{10^{n(pK_a - pH)} + 1} \quad (3)$$

where f_d is the fraction of the total simulation that the titratable residue spent in a deprotonated state.

Table 2 shows the calculated pK_a values for each titratable residue calculated from eq 3 for select exchange attempt frequencies. Hill coefficients that differ significantly from 1 imply either that the pK_a of that residue displays significant non-Henderson–Hasselbalch (non-HH) behavior or that protonation space is poorly sampled at some pH values, depending on how well eq 3 fits the data. If eq 3 fits the data poorly, then poor protonation state sampling is at least partially responsible for the deviation of the Hill coefficient from 1. Only the CpHMD simulations show several residues whose Hill coefficient deviates substantially from 1, showing that pH-REMD improves sampling from the desired ensemble.

Table 2. pK_a and Hill Coefficients for Each Residue Taken from Each Set of Simulations[a]

	CpHMD		EAF = 0.5 ps^{-1}		EAF = 50.0 ps^{-1}		
residue	pK_a	n	pK_a	n	pK_a	n	expt pK_a
Glu 7	3.62	1.16	3.60	0.88	3.84	0.96	2.6 ± 0.2
His 15	5.96	1.05	5.74	1.09	5.90	0.97	5.5 ± 0.2
Asp 18	2.26	1.11	2.01	0.94	2.01	0.89	2.8 ± 0.3
Glu 35	5.67	3.82	5.44	1.16	4.98	0.98	6.1 ± 0.4
Asp 48	1.22	0.43	1.11	0.71	1.99	0.83	1.4 ± 0.2
Asp 52	2.69	1.16	2.37	0.96	2.30	0.75	3.6 ± 0.3
Asp 66	−18.13	0.11	−3.17	0.49	1.53	1.19	1.2 ± 0.2
Asp 87	2.52	0.81	2.61	0.81	2.66	0.91	2.2 ± 0.1
Asp 101	3.69	2.10	3.66	1.00	3.57	0.87	4.5 ± 0.1
Asp 119	2.26	0.98	2.73	1.04	2.43	0.96	3.5 ± 0.3
rmse	**6.15 (0.74)**		**1.56 (0.76)**		**0.89**		

[a]The pK_a's and Hill coefficients (n) are shown for each EAF. pK_a root mean square errors (rmse's) from the ^{13}C-NMR experimental values published by Webb et al.[22] are shown in bold in the last row. Asp 66 was problematic because it is positioned between several Arginine residues, causing it to resist protonation. When it significantly impacts the rmse, the rmse for all residues except Asp 66 is shown in parentheses next to the total rmse.

4.3. Enhancing Protonation State Sampling with pH-REMD. Replica exchange methodologies are well-known to improve sampling in the desired ensemble[23,25] as long as replicas traverse the state-space ladder regularly. If replica exchange attempts always fail, the simulation does not benefit from those attempts. In our pH-REMD simulations, replicas with neighboring pH values (i.e., replicas with solution pH's separated by 0.5 pH units) succeeded between 40% and 98% of all exchanges attempted between adjacent replicas, displaying very efficient traversal of the pH-space replica ladder. Here, we will discuss the extent to which pH-REMD, with different exchange attempt frequencies (EAFs), improves protonation state sampling as compared to CpHMD.

We show sample titration curves for simulations with no exchange attempts and simulations in which replica exchanges were attempted with a frequency of 50 ps^{-1}. Residues for which "good" titration curves are obtained with CpHMD are shown in Figure 2. We characterize "good" titration curves by small deviations of each point from the fitted titration curve and Hill

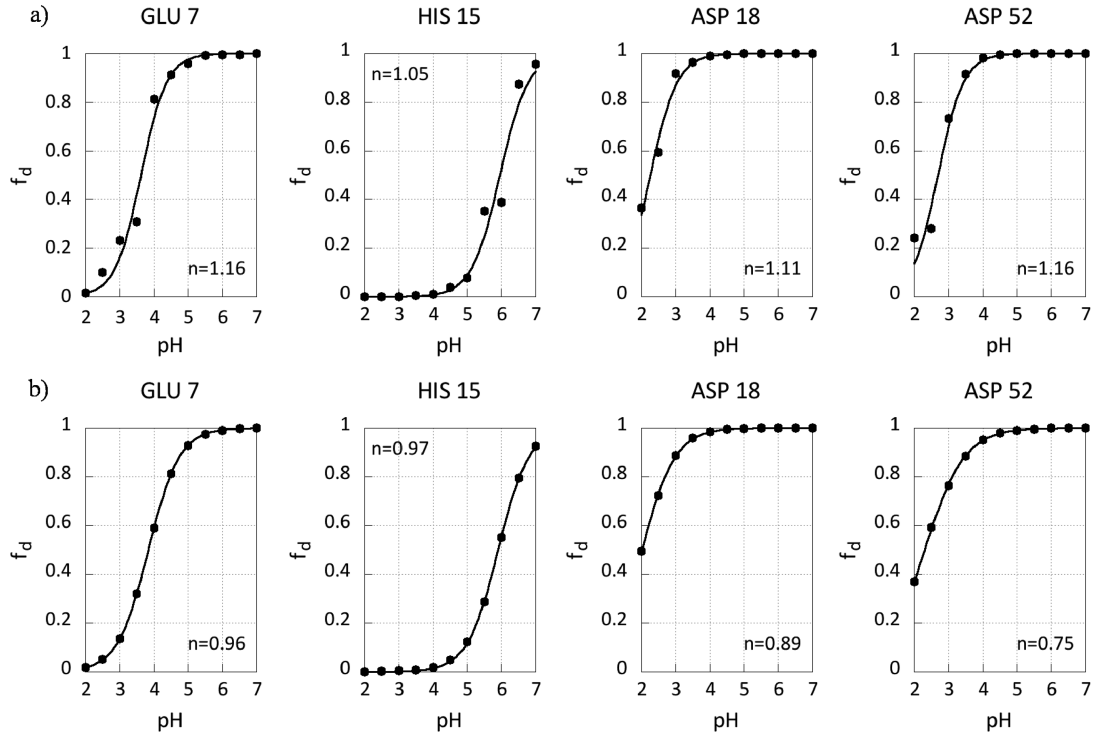

Figure 2. Titration curves obtained with (a) EAF = 0 ps^{-1} and (b) EAF = 50 ps^{-1}. The data for these residues show the best fit to eq 3 for the CpHMD simulations.

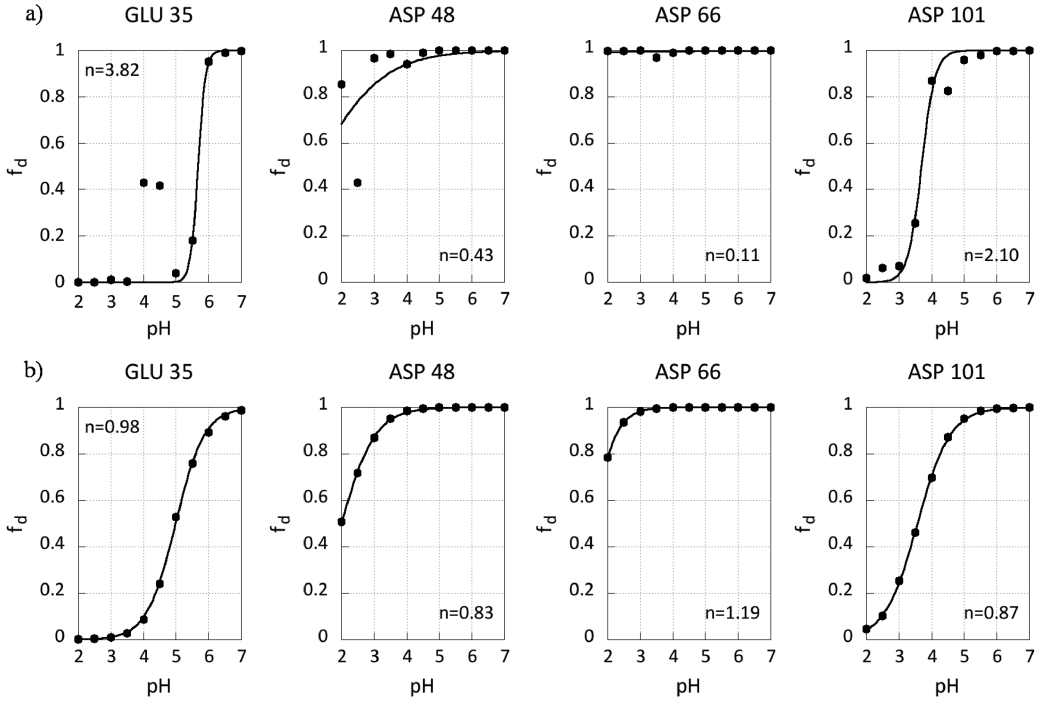

Figure 3. Titration curves obtained with (a) EAF = 0 ps^{-1} and (b) EAF = 50 ps^{-1}. The data for these residues have the poorest fit to eq 3 for the CpHMD simulations.

coefficients between 0.5 and 1.5. Residues that show poor titration curves for CpHMD, characterized by large deviations of points from the fitted titration curve and/or Hill coefficients significantly shifted from 1, are shown in Figure 3.

Figure 2 shows that even when CpHMD generates data that closely fit eq 3, using pH-REMD still improves the fit. A more drastic improvement is shown in Figure 3 where CpHMD performs poorly because some residues become conformationally trapped at several pH's, impacting protonation state sampling and skewing the points away from the titration curve.

The quality of the fits can be quantified by measuring the deviation of each point from the fitted equation according to eq 4:

dx.doi.org/10.1021/ct300512h | J. Chem. Theory Comput. 2012, 8, 4393−4404

$$RSS = \sum_{\text{points}} (O(x) - E(x))^2 \quad (4)$$

where RSS is the residual sum of squares, $O(x)$ is the actual data point, and $E(x)$ is the value of the fitted equation at that value of x. Equation 4 provides an easy way to quantitatively evaluate how well the titration data from the pH-REMD simulations fit eq 3 as compared to the CpHMD simulations. The results for the 8 residues plotted in Figures 2 and 3 are shown in Table 3.

Table 3. Value of *RSS* According to Equation 4 for the Eight Residues Shown in Figures 2 and 3[a]

residue	*RSS* (CpHMD)	*RSS* (EAF = 50 ps^{-1})
Glu 7	2.7×10^{-2}	7.9×10^{-5}
His 15	3.8×10^{-2}	2.7×10^{-5}
Asp 18	6.3×10^{-3}	3.3×10^{-5}
Asp 52	2.2×10^{-2}	1.3×10^{-3}
Glu 35	3.6×10^{-1}	4.2×10^{-4}
Asp 48	1.7×10^{-1}	2.4×10^{-5}
Asp 66	8.2×10^{-4}	2.9×10^{-4}
Asp 101	3.4×10^{-2}	2.7×10^{-4}

[a]Larger values represent more deviation from the fitted curve, whereas a value of 0 represents a perfect fit. The "good" titratable residues (Figure 2) are the first four entries, and the "bad" titratable residues (Figure 3) are the last four entries.

The improvement by using pH-REMD over conventional CpHMD, already apparent by viewing Figures 2 and 3, is striking as measured in Table 3. Even when CpHMD performs well, pH-REMD results in an improvement of 2−3 orders of magnitude in the *RSS* metric, and results in at least another order of magnitude of improvement in the cases where CpHMD performs poorly (except for Asp 66, for which CpHMD has already proven to perform poorly in this study).

By exchanging structures with other replicas, ensembles generated at each pH in pH-REMD simulations are able to escape from local minima that prevent titratable residues from accurately sampling protonation states. Because each replica is run independently, snapshots in each replica are not correlated with one another, so ensembles generated at each pH contain more uncorrelated members in simulations with more rapid EAFs (as long as replica exchange attempts succeed regularly). Therefore, pH-REMD's ability to cross free energy barriers more efficiently reduces to an entropy argument; ensembles at each pH are given more opportunities to sample different conformations.

Another way of thinking about pH-REMD simulations is to consider the entire expanded ensemble, in which the simulations sample in both conformational-space and pH-space. CpHMD simulations, on the other hand, do not sample in pH-space, as the pH remains constant throughout the entire simulation. The protonation state of each titratable residue strongly depends on both the solution pH and the protein conformation and is coupled to other titratable residues in complicated ways. Therefore, pH-REMD simulations can move through a larger free energy space extended to another dimension relative to CpHMD simulations, pH-space. CpHMD simulations are unable to take advantage of lower free energy barriers in this expanded ensemble, causing them to become more easily trapped in conformations that skew predicted pK_a's as compared to pH-REMD simulations.

In an extreme case, Asp 66, the CpHMD simulations at low pH never visited conformations favorable to protonating. By allowing exchanges between pH replicas, ensembles at lower pH crossed into regions of phase space favorable to Asp 66 protonation.

The case of Asp 66 further demonstrates that increasing the EAF improves protonation state sampling. The pK_a prediction systematically improves as EAF is increased, and the Hill coefficient improves from 0.11 to 1.19.

5. EXCHANGE ATTEMPT FREQUENCY AND PROTONATION STATE SAMPLING

To analyze the effect EAF has on pK_a convergence, we divided each simulation into sections of 0.25 ns and calculated the standard deviations of the pK_a and Hill coefficient, as well as the mean Hill coefficient, by fitting eq 3 to the data obtained from each pH. The results are summarized in Table 4.

The average fluctuation in pK_a systematically decreases as EAF increases, in large part due to the improvement of residues that titrate poorly, Asp 48 and Asp 66. The large standard deviation of these two residues is evidence that the protonation state sampling does not converge on the 0.25 ns intervals that

Table 4. Standard Deviations of pK_a (σ_{pK_a}) and Hill Coefficient (σ_n) and Average Hill Coefficient ($\bar{n}$) Calculated by Dividing Each Simulation into Sections of 0.25 ns[a]

	CpHMD			EAF = 50.0 ps^{-1}			EAF = 0.5 ps^{-1}		
residue	σ_{pK_a}	$\bar{n}$	σ_n	σ_{pK_a}	$\bar{n}$	σ_n	σ_{pK_a}	$\bar{n}$	σ_n
Glu 7	0.18	3.1	3.3	0.29	1.0	0.2	0.15	1.0	0.1
His 15	0.24	2.6	1.7	0.21	1.2	0.4	0.20	1.0	0.1
Asp 18	0.27	1.4	0.7	0.29	1.0	0.3	0.28	1.0	0.3
Glu 35	0.42	8.1	6.7	0.30	1.6	0.6	0.41	1.2	0.3
Asp 48	6.61	1.8	3.5	5.1	1.0	1.2	3.3	1.1	0.8
Asp 52	1.04	1.2	0.8	0.40	1.2	0.5	0.64	1.0	0.7
Asp 66	15	0.8	0.9	15	1.0	0.3	4.9	1.4	0.9
Asp 87	0.42	2.0	1.8	0.37	1.0	0.4	0.43	1.1	0.3
Asp 101	0.20	3.8	2.1	0.19	1.1	0.2	0.30	0.7	0.2
Asp 119	0.33	1.4	0.8	0.22	1.2	0.3	0.24	1.1	0.3
average	2.4	3.0	2.7	2.2	1.1	0.4	1.1	1.1	0.4

[a]The pK_a and Hill coefficients are calculated for each section of the simulation by fitting data from all pH replicas to eq 3 and calculating the statistics from the 60 resulting data points.

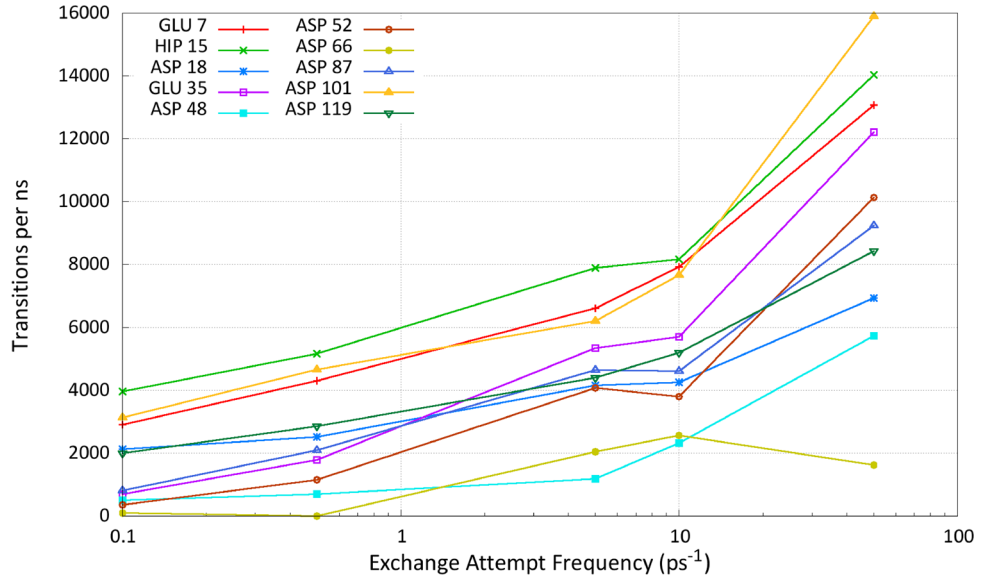

Figure 4. Number of protonation state transitions per nanosecond of simulation time. A transition is counted if consecutive snapshots in the ensemble have a different number of protons for that residue. The CpHMD results are labeled with EAF = 0.1 ps^{-1} to fit on the log-scale.

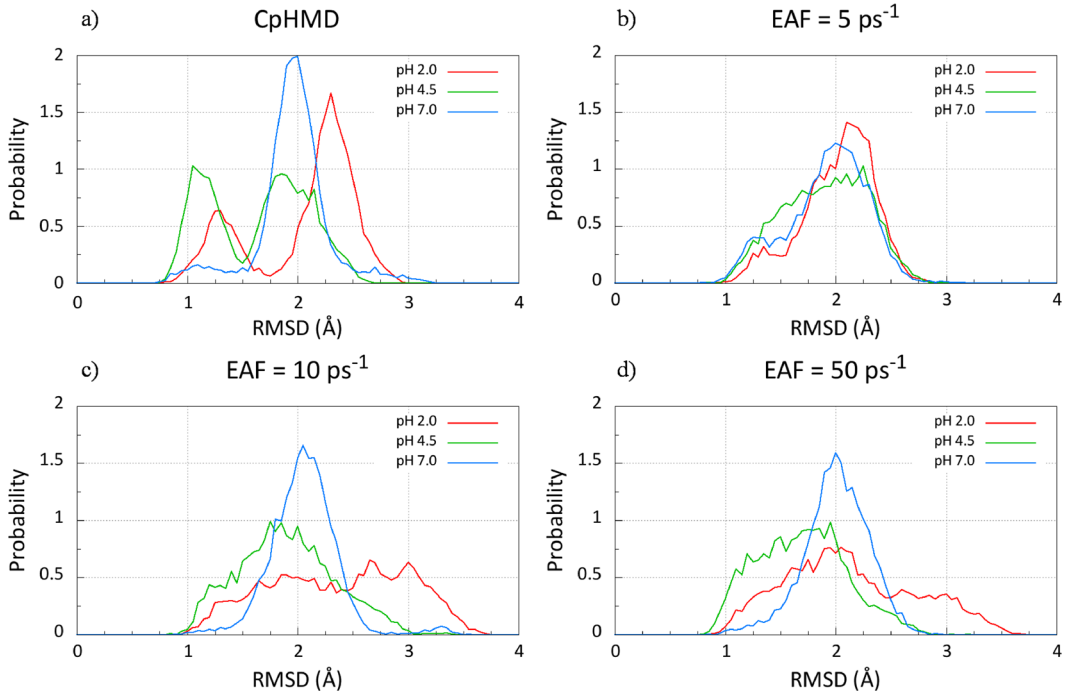

Figure 5. Histogrammed RMSD data for pH 2, pH 4.5, and pH 7 taken from simulations run with different EAFs.

were used to generate the statistics. However, increasing the EAF leads to a systematic decrease in the fluctuations of the calculated pK_a for Asp 48 and Asp 66, because a higher EAF decreases the simulation time required to achieve pK_a convergence.

The trend of the Hill coefficient shown in Table 4 also shows a radical improvement in protonation state sampling with pH-REMD. While a Hill coefficient that deviates significantly from 1 may indicate cooperativity between titrating residues, previous evidence suggests these residues mostly titrate independently.[16] Furthermore, because CpHMD and pH-REMD simulations converge to the same limiting ensemble, Hill coefficients that diverge significantly from 1 in CpHMD simulations but remain close to 1 in the pH-REMD simulations most likely indicate poor protonation state sampling in the CpHMD simulations.

The CpHMD simulations show an average Hill coefficient of at least 2 for one-half of the titratable residues, and its standard deviations are nearly as large as the Hill coefficient itself. In this case, even low EAFs result in Hill coefficients closer to 1, and their average relative standard deviation drops from 100% to 33%. Therefore, the Hill coefficients from the CpHMD simulations symbolize poor protonation state sampling rather than strong cooperativity between titrating residues.

A final metric for analyzing protonation state sampling of a particular residue is to count the number of times the

dx.doi.org/10.1021/ct300512h | J. Chem. Theory Comput. 2012, 8, 4393−4404

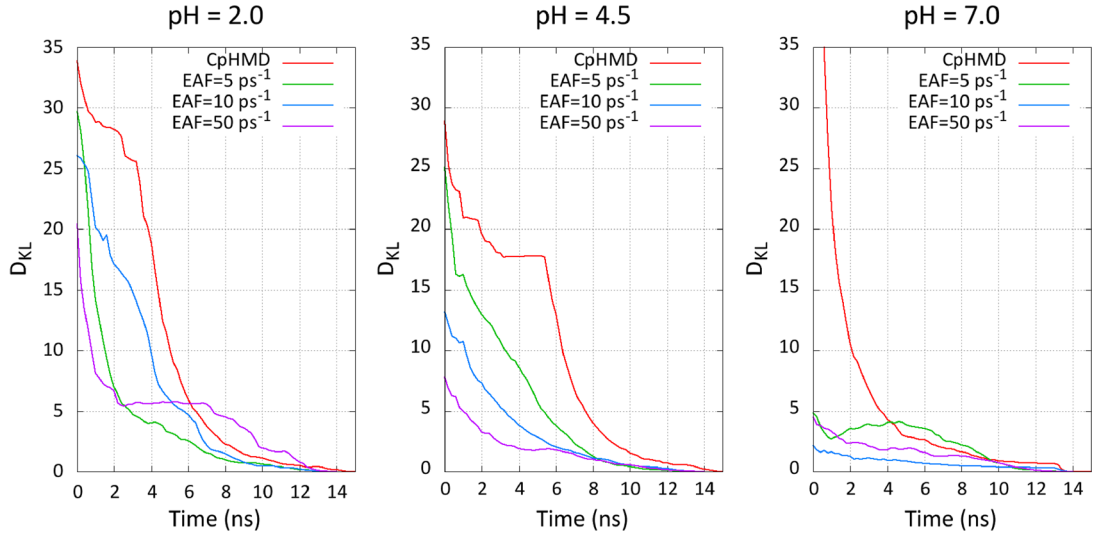

Figure 6. Kullback–Leibler divergence for each simulation calculated via eq 5. $P(i)$ is the RMSD histogram of the indicated simulation at time t, and $Q(i)$ is the RMSD histogram of the entire indicated simulation. Values closer to zero indicate distributions of higher similarity.

protonation state changes over a specified period of time. We call these protonation state changes transitions, and we only consider a transition to have occurred if the number of protons on the titratable side-chain changed from one snapshot to the next in a given ensemble. In particular, a tautomeric change, such as a proton changing from one oxygen in a carboxylate to the other oxygen, is not counted. Figure 4 shows how the number of protonation state transitions per nanosecond of simulation, summed over every replica from pH 2 to 7, changes with EAF. In every simulation, protonation state changes are attempted every five steps.

Simulations that result in more transitions demonstrate enhanced protonation state sampling, because more protonation state changes occur in the same amount of time. All simulations were carried out with the same set of parameters so every ensemble generated at a given pH will converge to the same result given enough simulation time. Therefore, simulations with more transitions will obtain converged pK_a values faster.

Figure 4 shows that increasing EAF dramatically increases the number of transitions despite the fact that the frequency of attempted protonation state changes is constant. This is due to the nature of the probability of accepting a replica exchange attempt, which is governed by eq 2. Because the success of an exchange attempt depends only on the net difference of titrating protons between the two replicas, it is possible for this net difference to be small; therefore, the probability of accepting the exchange attempt is large, even when several residues have different protonation states. Therefore, numerous protonation state changes for individual residues often accompany a successful exchange of replicas.

5.1. Enhancing Conformational State Sampling with pH-REMD. Because conformations and protonation states are coupled, enhanced conformational sampling from pH-REMD naturally accompanies enhanced protonation state sampling. In well-designed pH-REMD simulations (i.e., pH-REMD simulations in which efficient mixing occurs in pH-space), each replica contributes structures to the ensemble at each pH, which serves to increase the number of conformations visited at each pH.

The RMSD is a metric that reflects how different the sampled conformations are from a reference, in this case, the original, minimized crystal structure. The histogrammed RMSD data from Figure 1 are shown in Figure 5 to allow easier comparison between the different simulations.

Simulations with higher EAFs traverse the replica ladder more rapidly, allowing trajectories to break out of local minima that are tied to a particular protonation state. The widening bin-widths in Figure 5 show that RMSD-space is explored more thoroughly within the 15 ns time scale sampled in each simulation as EAF increases to 10 ps^{-1} (there is no noticeable difference between the 10 and 50 ps^{-1} EAF).

Because each simulation is subjected to the same set of external constraints (e.g., temperature, pH, solvation model, etc.), each generated ensemble should represent a subset of the theoretically complete ensemble under these external constraints. Because these wider RMSD distributions reflect sampling of more conformations further from the starting structure, it is almost certain that these wider distributions at high EAF are thermodynamically "better" (i.e., the ensembles approximate the theoretically complete ensembles better) than their narrower counterparts in the CpHMD and 5 ps^{-1} EAF simulations. The original RMSD data, plotted in Figure 1, also suggest that pH-REMD simulations converge more rapidly because those simulations display many transitions between conformations with different RMSD's.

In addition to sampling more RMSD space than CpHMD simulations, the pH-REMD simulations also converge to their final RMSD distributions much more rapidly. To quantify this measure, we used the Kullback–Leibler divergence[42,43] (D_{KL}). The Kullback–Leibler divergence, calculated via eq 5, quantifies the similarity between two distinct probability distributions $P(i)$ and $Q(i)$.

$$D_{KL} = \sum_{i=1}^{N} P(i) \ln\left(\frac{P(i)}{Q(i)}\right) \quad (5)$$

where D_{KL} is the Kullback–Leibler divergence metric, i is the property of interest (RMSD in this case), and $P(i)$ and $Q(i)$ are two probability distribution functions on i-space. For discrete spaces (such as those obtained by histogramming data), eq 5 is

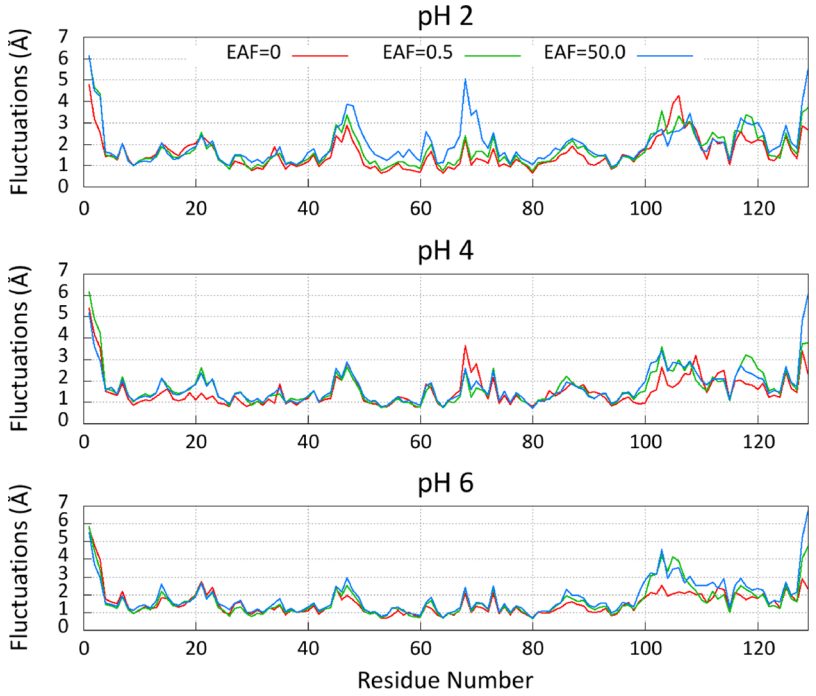

Figure 7. Average atomic fluctuations for each residue relative to the average structure of the ensemble. Data are shown for CpHMD, low EAF (0.5 ps^{-1}), and high EAF (50 ps^{-1}).

represented as a sum (as shown), but becomes an integral over all of i-space for continuous probability distribution functions $P(i)$ and $Q(i)$.

Figure 6 plots D_{KL} calculated from eq 5 where $P(i)$ is the RMSD distribution of each simulation at time t and $Q(i)$ is the final RMSD distribution of each simulation. As $P(i)$ and $Q(i)$ become more similar, D_{KL} tends toward zero. Therefore, the curves that approach zero more rapidly approach their final RMSD distribution in a shorter amount of time.

The pH-REMD simulations not only explore more RMSD space than the corresponding CpHMD simulations, but they characterize this larger space more rapidly as well, because they converge to their final distribution faster than CpHMD. Furthermore, the simulations with an EAF of 10 and 50 ps^{-1} typically converge faster than the one with an EAF of 5 ps^{-1}. The only exception in this case, including the pH's not shown in Figure 6, is the simulation at pH 2. In general, simulations with EAF 10 and 50 ps^{-1} are indistinguishable with respect to RMSD.

At pH 2, the RMSD distribution of the EAF = 5 ps^{-1} simulation is much narrower than the corresponding distributions at EAF 10 and 50 ps^{-1}. Therefore, it is not surprising that the D_{KL} of the 5 ps^{-1} EAF simulation converges more rapidly than the higher EAFs. In general, however, pH-REMD simulations with high EAFs sample more RMSD space more efficiently than do CpHMD and simulations with low EAFs.

To probe the nature of the conformational flexibility of HEWL at different EAFs, we calculated the average atomic fluctuations for each residue from the average structure. These fluctuations provide insight into the flexible regions of the protein, giving a more fine-grained, structural analysis than does RMSD. The results, shown in Figure 7, show that the same parts of HEWL are generally flexible for each simulation, but the pH-REMD simulations tend to display enhanced flexibility as compared to the CpHMD simulations. Again, because each simulation samples from the same ensemble subject to the same thermodynamic constraints, this increased flexibility suggests that the simulations at high EAF converge to the true ensemble more rapidly than do the CpHMD simulations and the pH-REMD simulations with a low EAF.

While the overall flexibility in pH-REMD simulations is increased with respect to the CpHMD simulations, the dynamics still reveal different behavior at different pH's. In particular, the region between residues 100 and 120 shows drastically increased flexibility at pH values higher than 4 for the pH-REMD as compared to the CpHMD simulations.

Furthermore, the region around residue 70, which shows heightened flexibility at pH 2 (Figure 7), contains the problematic titratable residue Asp 66. This increased flexibility at high EAF is the likely explanation why Asp 66 protonates at low pH in the pH-REMD simulations but not in the CpHMD simulation where this loop is substantially less flexible.

To probe the pH-dependence of HEWL dynamics further, we plot the distributions of the distance between the carboxylate carbons of the catalytic residues Asp 52 and Glu 35 at each pH. Because Asp 52 and GLU 35 are the catalytic residues in HEWL, this behavior may have important implications in the HEWL catalytic activity profile as a function of pH.

Figure 8 shows that only the simulation run at pH 5 samples conformations in which Asp 52 and Glu 35 are closely interacting for the CpHMD simulations. Furthermore, the simulation at pH 5 spends roughly 75% of its time "stuck" in this close interaction. It is highly unlikely that this interaction is so strong at pH 5, yet is almost nonexistent at pH 4.5 and 5.5. More likely, Figure 8 suggests that the CpHMD simulation run at pH 5 became trapped, while trajectories at other pH values were unable to enter this conformational bin within the 16 ns of simulation.

pH-REMD simulations with a high EAF easily overcome this barrier within the simulation time scale. The distributions from

dx.doi.org/10.1021/ct300512h | J. Chem. Theory Comput. 2012, 8, 4393−4404

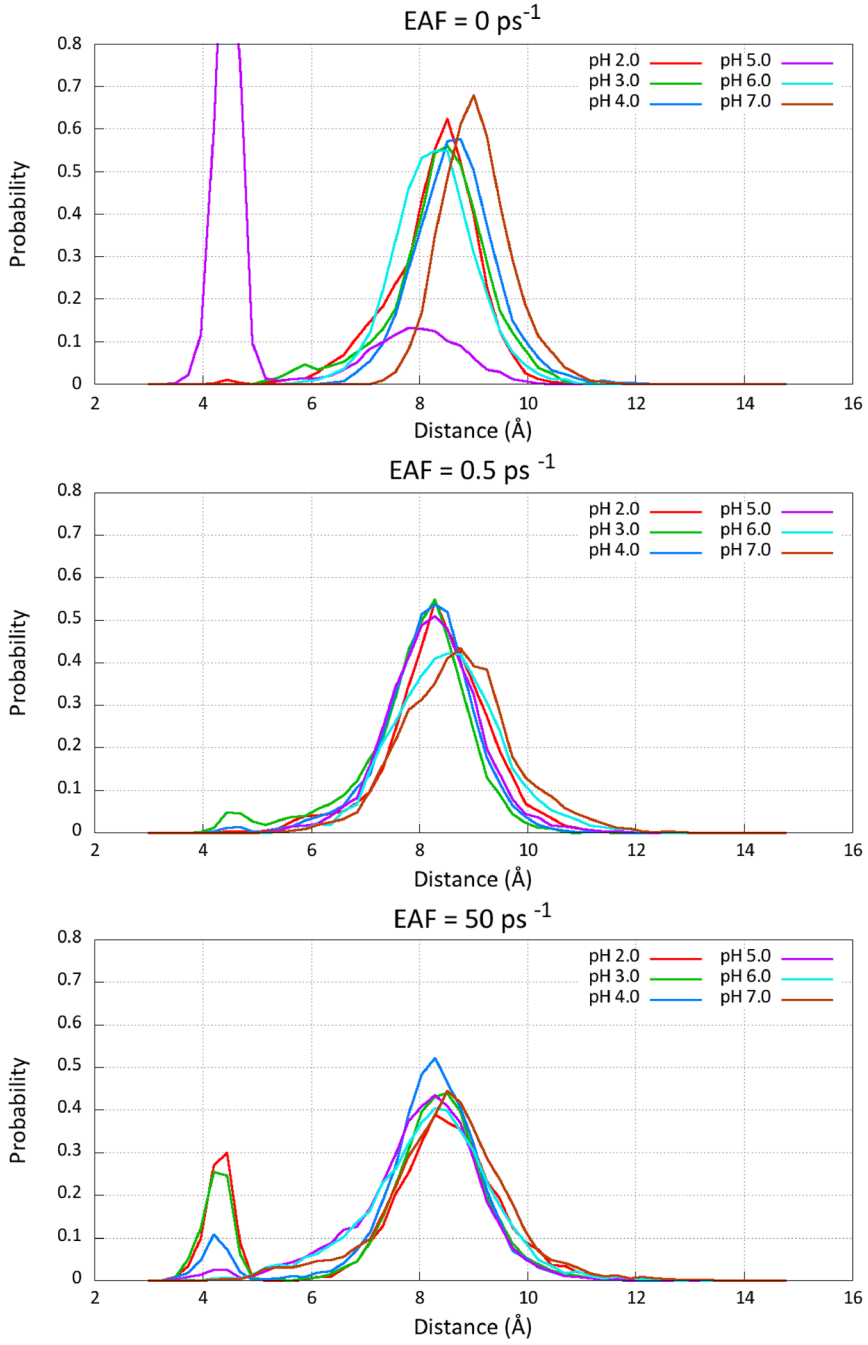

Figure 8. Distributions of the Asp52-C^{γ}−Glu35-C^{δ} carboxylate carbons. Asp 52 and Glu 35 are the catalytic residues of HEWL.

pH-REMD simulations with a 50 ps^{-1} EAF display more expected behavior, given that the calculated pK_a's of Asp 52 and Glu 35 are 2.30 and 4.98, respectively (Table 2). This interaction is likely strongest when one of the carboxylates is protonated and the other is deprotonated, and it is likely weakest when both are deprotonated. Therefore, this interaction should be strongest at a pH between 2.30 and 4.98.

The Asp 52−Glu 35 interaction is the strongest at pH 2.5 and decays as the pH either increases or decreases. At pH 2.5, Asp 52 is most likely deprotonated, while Glu 35 is most likely protonated. At pH 2.0, both residues are likely to be protonated, resulting in a slightly weaker interaction. However, this is still more favorable than when both residues are deprotonated, so the interaction becomes significantly weaker as the pH increases.

Furthermore, tight coupling between Asp 52 and Glu 35 likely induces non-HH behavior as these residues no longer titrate independently. This explains why the Hill coefficient for Asp 52, reported in Table 2, is more significantly shifted away from 1, to 0.75, for the EAF of 50 ps^{-1} . Over the pH range that contains the Asp 52 inflection point, 8 shows that the interaction between the two active site residues is strong. Over the pH range that contains the Glu 35 inflection point, however, the interaction is weak, causing the Glu 35 titration to display nearly ideal Henderson−Hasselbalch behavior.

To better illustrate the pH-dependence of the Glu 35−Asp 52 interaction depicted in Figure 8 (at 50 ps^{-1} EAF), we

dx.doi.org/10.1021/ct300512h | J. Chem. Theory Comput. 2012, 8, 4393−4404

integrated each of the distributions from 0 to 5 Å and plotted the result against pH, shown in Figure 9.

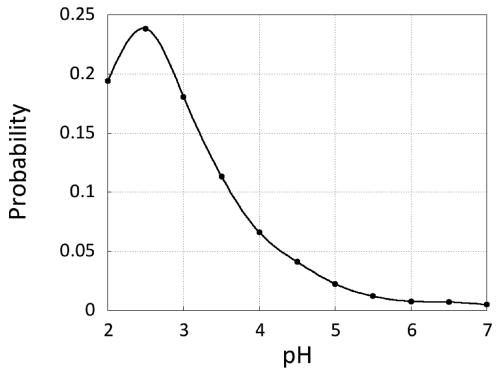

Figure 9. Fraction of simulation with the Glu 35−Asp 52 distance shorter than 5 Å versus pH.

5.2. Scalability with Increasing Exchange Attempt Frequency. It is important when selecting a simulation protocol to consider the performance implications of each of the choices, because there is often a trade-off between computational expense and theoretical rigor. As Mongan et al. demonstrated in their work, the CpHMD method implemented in AMBER is only marginally more expensive than traditional MD with constant protonation states.[16] Here, we will discuss the performance implications of increasing the EAF of pH-REMD simulations.

The computational cost of the pH-REMD simulations is the sum of the cost of the underlying CpHMD method[16] and the cost of the replica exchange attempts. The exchange success probability in pH-REMD simulations is governed by eq 2 and can be implemented so that the computational cost of each exchange attempt is negligible. The replicas of every simulation were carried out on 24 processors on NICS Keeneland,[44] so the simulation efficiency, measured in terms of nanosecond of simulation per day, can be directly compared. The average results obtained for each EAF are summarized in Table 5.

Table 5. Average Timings for CpHMD and pH-REMD Simulations[a]

EAF (ps^{-1})	efficiency (ns/day)
0.0	7.56
0.5	6.81
5.0	6.55
10.0	6.72
50.0	6.70

[a]CpHMD simulations used 24 processors, whereas pH-REMD simulations used 288 processors, 24 per replica. All simulations were performed on NICS Keeneland.[44]

The decreased performance from the CpHMD simulation (EAF = 0.0 in Table 5) to the EAF = 5.0 ps^{-1}simulations arises from the fact that REMD simulations in AMBER currently require each replica to perform the same number of MD steps between exchange attempts. This synchronization causes each replica to run only as fast as the slowest replica.

The pH-REMD simulations are run with 288 processors (12 replicas with 24 processors each), whereas the CpHMD simulations are run each replica independently, with only 24 processors. Therefore, the synchronization of the replicas in REMD is responsible for the 10% performance reduction between the CpHMD simulation and the pH-REMD simulation with an EAF of 0.5 ps^{-1} (attempting exchanges every 1000 integration steps).

Increasing the EAF of pH-REMD simulations from 0.5 to 50.0 ps^{-1} (attempting exchanges every 10 steps) results in a 1% reduction in average simulation efficiency, a value that falls well within the fluctuations between two different simulations with the same EAF run on the same machine. Given the lack of performance degradation as EAF increases and the improved performance of simulations as EAF increases, the best EAF to use with the presented pH-REMD implementation is one where exchanges are attempted every 10−50 integration steps (10.0 and 50.0 ps^{-1} in this study, respectively).

6. CONCLUSION

In this study, we have shown that pH-REMD effectively enhances sampling from the semigrand canonical ensemble as compared to CpHMD in the case of hen egg white lysozyme. The titration curves generated from pH-REMD simulations are considerably less noisy than the analogous titration curves generated from CpHMD simulations, and they fit to the Hill equation much better. Furthermore, pK_a's calculated from pH-REMD simulations converge faster and achieve better precision than CpHMD.

In some cases, pH-REMD can effectively cross potential energy barriers that trap residues in CpHMD simulations. In the case of the Asp 66 residue in HEWL, CpHMD simulations were unable to obtain noticeable protonation fractions even at a pH as low as 2 when starting from the 1AKI crystal structure. Utilizing pH-REMD simulations with a rapid EAF, we obtained a titration curve with a Hill coefficient close to 1 and a calculated pK_a that compares well to experiment.

We have demonstrated that increasing the EAF improves sampling and convergence of several observables in this study. Asp 66 titrates more efficiently with a high EAF due to the nhanced mobility of flexible regions of the protein. Furthermore, analysis of the distance between the catalytic residues Asp 52 and Glu 35 shows that increasing the EAF can provide valuable chemical insight into biologically significant pH-dependent behavior of proteins. Similar to past work with temperature REMD,[31,32] high EAFs give rise to more rapid convergence.

Replica exchange methodologies can be implemented efficiently to reduce the cost of each exchange attempt. In pH-REMD, the exchange success probability, governed by eq 2, involves only trivial mathematics, so the cost of evaluating eq 2 is negligible. For efficient REMD implementations, like the one presented in this work, we recommend setting the EAF to at least 10 ps^{-1}, although some improvement is still seen with higher EAFs.

Chodera and Shirts[25] provide an explanation for the improved efficiency of high EAFs by relating it to Gibbs' sampling and the effect high EAF has on "state space" sampling (pH-space in this study). In their paper, Chodera and Shirts propose enhancements to the exchange process in REMD simulations, such as exchanges between nonadjacent neighbors in "state space" as well as attempting multiple exchanges before resuming dynamics.[25]

pH-REMD is likely to benefit by attempting exchanges between nonadjacent neighbors, because the difference in pH between replicas is small. Given the simplicity of the exchange probability equation (eq 2), the exchange success rate can be

calculated between any two replicas over the course of the pH-REMD simulation. The calculated success rates show a non-negligible probability of accepting exchange attempts between replicas up to 2 pH units away from each other (i.e., separated by 3 replicas).

In future work, we plan to implement Gibbs' sampling techniques[25] into the REMD exchange attempt process in AMBER to improve the efficiency of pH-REMD. We will also extend the CpHMD and pH-REMD methods presented here to simulations in explicit solvent, which has proven effective in continuous protonation state models.[29]

AUTHOR INFORMATION

Corresponding Author

*E-mail: roitberg@ufl.edu.

Notes

The authors declare no competing financial interest.

ACKNOWLEDGMENTS

J.M.S. gratefully acknowledges support from the NSF GRFP award. We thank Natali Di Russo, Bill Miller III, and Juan Bueren Calabuig for critical reading and constructive feedback on the manuscript. We also thank Darrin York for helpful and encouraging discussions about pH-REMD.

REFERENCES

(1) Itoh, S. G.; Damjanović, A.; Brooks, B. R. *Proteins* **2011**, *79*, 3420−3436.
(2) Cornish-Bowden, A. J.; Knowles, J. R. *Biochem. J.* **1969**, *113*, 353−362.
(3) White, F. H., Jr.; Anfinsen, C. B. *Ann. N. Y. Acad. Sci.* **1959**, *81*, 515−523.
(4) Tanford, C.; Kirkwood, J. G. *J. Am. Chem. Soc.* **1957**, *79*, 5333−5339.
(5) Olsson, M. H. M.; Söndergaard, C. R.; Rostkowski, M.; Jensen, J. H. *J. Chem. Theory Comput.* **2011**, *7*, 525−537.
(6) Myers, J.; Grothaus, G.; Narayanan, S.; Onufriev, A. *Proteins* **2006**, *63*, 928−938.
(7) Bashford, D.; Karplus, M. *Biochemistry* **1990**, *29*, 10219−10225.
(8) Bashford, D.; Gerwert, K. *J. Mol. Biol.* **1992**, *224*, 473−486.
(9) Antosiewicz, J.; McCammon, J.; Gilson, M. K. *J. Mol. Biol.* **1994**, *238*, 415−436.
(10) Song, Y.; Mao, J.; Gunner, M. R. *Biophys. J.* **2009**, *72*, 2075−2093.
(11) Baptista, A. M.; Martel, P. J.; Petersen, S. B. *Proteins* **1997**, *27*, 523−544.
(12) Baptista, A. M.; Teixeira, V. H.; Soares, C. M. *J. Chem. Phys.* **2002**, *117*, 4184.
(13) Bürgi, R.; Kollman, P. A.; Gunsteren, W. F. v. *Proteins* **2002**, *47*, 469−480.
(14) Lee, M. S.; F. R., S., Jr.; C. L., B., III. *Proteins* **2004**, *56*, 738−752.
(15) Börjesson, U.; Hünenberger, P. H. *J. Phys. Chem. B* **2004**, *108*, 13551−13559.
(16) Mongan, J.; Case, D.; McCammon, A. *J. Comput. Chem.* **2004**, *25*, 2038−2048.
(17) Khandogin, J.; Brooks, C. L. *Biophys. J.* **2005**, *89*, 141−157.
(18) Alexov, E.; Mehler, E. L.; Baker, N.; Baptista, A.; Huang, Y.; Milletti, F.; Nielsen, E. J.; Farrell, D.; Carstensen, T.; Olsson, M. H. M.; Shen, J. K.; Warwicker, J.; Williams, S.; Word, J. M. *Proteins* **2011**, *79*, 3260−3275.
(19) Machuqueiro, M.; Baptista, A. M. *Proteins* **2011**, *79*, 3437−3447.
(20) Hamelberg, D.; Mongan, J.; McCammon, J. A. *J. Chem. Phys.* **2004**, *120*, 11919−29.
(21) Williams, S.; de Oliveira, C.; McCammon, J. *J. Chem. Theory Comput.* **2010**, *6*, 560−568.
(22) Webb, H.; Tynan-Connolly, B. M.; Lee, G. M.; Farrell, D.; O'Meara, F.; Söndergaard, C. R.; Teilum, K.; Hewage, C.; McIntosh, L. P.; Nielsen, J. E. *Proteins* **2011**, *79*, 685−702.
(23) Sugita, Y.; Okamoto, Y. *Chem. Phys. Lett.* **1999**, *314*, 141−151.
(24) Pitera, J. W.; Swope, W. *Proc. Natl. Acad. Sci. U.S.A.* **2003**, *100*, 7587−7592.
(25) Chodera, J. D.; Shirts, M. R. *J. Chem. Phys.* **2011**, *135*, 194110.
(26) Nadler, W.; Meinke, J. H.; Hansmann, U. H. E. *Phys. Rev. E* **2008**, *78*, 061905.
(27) Meng, Y.; Roitberg, A. E. *J. Chem. Theory Comput.* **2010**, *6*, 1401−1412.
(28) Meng, Y.; Dashti, D. S.; Roitberg, A. E. *J. Chem. Theory Comput.* **2011**, *7*, 2721−2727.
(29) Wallace, J. A.; Shen, J. K. *J. Chem. Theory Comput.* **2011**, *7*, 2617.
(30) Case, D. A.; et al. *AMBER 12*; 2012.
(31) Sindhikara, D.; Meng, Y.; Roitberg, A. E. *J. Chem. Phys.* **2008**, *128*, 024103−024103−10.
(32) Sindhikara, D. J.; Emerson, D. J.; Roitberg, A. E. *J. Chem. Theory Comput.* **2010**, *6*, 2804−2808.
(33) Sabri Dashti, D.; Meng, Y.; Roitberg, A. E. *J. Phys. Chem. B* **2012**, *116*, 8805−11.
(34) Takahashi, T.; Nakamura, H.; Wada, A. *Biopolymers* **1992**, *32*, 897−909.
(35) Bartik, K.; Redfield, C.; Dobson, C. M. *Biophys. J.* **1994**, *66*, 1180−1184.
(36) Demchuk, E.; Wade, R. C. *J. Phys. Chem.* **1996**, *100*, 17373−17387.
(37) Artymiuk, P. J.; Blake, C. C. F.; Rice, D. W.; Wilson, K. S. *Acta. Crystallogr., Sect. B* **1982**, *38*, 778−783.
(38) Hornak, V.; Abel, R.; Okur, A.; Strockbine, B.; Roitberg, A.; Simmerling, C. *Proteins* **2006**, *65*, 712−725.
(39) Onufriev, A.; Bashford, D.; Case, D. A. *Proteins* **2004**, *55*, 383−394.
(40) Vocadlo, D. J.; Davies, G. J.; Laine, R.; Withers, S. G. *Nature* **2001**, *412*, 835−838.
(41) Sindhikara, D. J.; Kim, S.; Voter, A. F.; Roitberg, A. E. *J. Chem. Theory Comput.* **2009**, *5*, 1624−1631.
(42) Hamacher, K. *J. Comput. Chem.* **2007**, *28*, 2576−2580.
(43) McClendon, C. L.; Hua, L.; Barreiro, G.; Jacobson, M. P. *J. Chem. Theory Comput.* **2012**, *8*, 2115−2126.
(44) Vetter, J. S.; Glassbrook, R.; Dongarra, J.; Schwan, K.; Loftis, B.; McNally, S.; Meredith, J.; Rogers, J.; Roth, P.; Spafford, K.; Yalamanchili, S. *Comput. Sci. Eng.* **2011**, *13*, 90−95.